Journal of Computational Electronics (2018) 17:586–594
https://doi.org/10.1007/s10825-018-1160-6

Electronic signature of single-molecular device based on polyacetylene derivative

Alexandre de S. Oliveira[1] · Antonio T. M. Beirão[1] · Shirsley S. da Silva[2] · Jordan Del Nero[3]

Published online: 28 March 2018

Abstract
We reported for polyacetylene chains containing $N = 6, 10, 20$ carbon atoms making bridges with gold electrodes which exhibit linear and nonlinear current/voltage signatures. The non-equilibrium quantum transport calculations are obtained from (1) low-voltage regime of 0–0.1 V and (2) high-voltage regime of 0–1.0 V. The nonlinear current/voltage behavior for high-voltage regime 0–1.0 V suggests that the system can operate as follows: (1) at 0.27 V there is a resonance captured by the I–V plot; (2) from 0.42 to 0.65 V a plateau is reached presenting a field effect transistor behavior; (3) there is a decrease in conductance from 0.66 V, and a negative differential resonance emerges with minimum value of 0.72 V. The linear I–V behavior will be reviewed, and we discuss the destructive quantum interference status. The effect occurs when we analyze the (1) low-voltage regime, and our results show that the conductance in oscillations maximizes the impact of quantum interferences (QI) on the I–V curve. In the present work, we demonstrate that QI in nanowire molecules is intimately related to the topology of the molecule's π system and establish the existence of QI-induced transmission antiresonances when different voltage regimes are triggered.

Keywords Polyacetylene · Field effect transistor (FET) · Low bias · High bias · Quantum interference · Destructive

1 Introduction

The use of conjugate polymers [1,2] as the conductive material and their potential as an electronic circuit element with nonlinear current–voltage characteristics at the nanoscale are well reported in the literature: these molecular wires are widely investigated in the study of transport properties at the single molecule [3,4].

Previous studies have shown that conjugated polymers may be conductors or semiconductors when doped [5]. Isoelectronic polymers such as polyethylene, polyamines and polyazomethine in neutral states and bipolaron are theoretically investigated in the ground and excited states showing high conductivity in unconventional one-dimensional devices [6].

Consistent theoretical models [7] that explore the characteristics of electronic transport in metal–molecule–metal devices are widely used. For the case of trans-polyacetylene coupled to two aluminum electrodes, it was possible to capture all the physical characteristics that appear in the transmittance curves [8]. On the other hand, we must take into account the effects of quantum interference in the electronic transport due to several directions of excitation along the single molecule [9,10]. It is the case of polycyclic aromatic hydrocarbon (PAHs) with multiple benzene rings coupled to polyenic chains with two possible *cis-trans* configurations in which the conductance depends on the point of contact in the loop and the configuration "cis" has destructive interference and "trans" constructive interference [11].

T-shaped and cyclic molecules qualitatively exhibit quantum interference (QI) more evidently in their transmission spectra [12].

Recently, features of the quantum interference were used to interpret the electron transport behavior in specific conjugate molecules [13] and even the appearance of QI in linear systems (1-D) [14] is responsible for QI signatures

✉ Alexandre de S. Oliveira
alexandrecn8@gmail.com

[1] Pós-graduação em Engenharia Elétrica, Universidade Federal do Pará, Belém, PA 66075-970, Brazil

[2] Faculdade de Física, Universidade Federal do Pará, Ananindeua, PA 67030-000, Brazil

[3] Faculdade de Física, Universidade Federal do Pará, Belém, PA 66075-110, Brazil

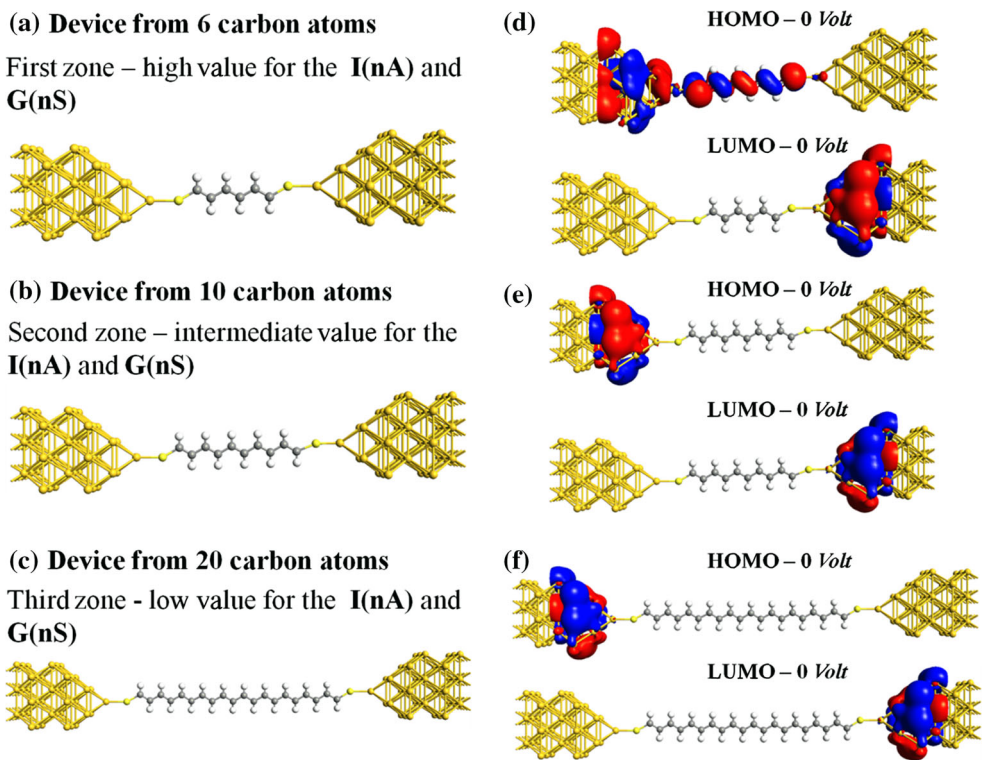

Fig. 1 Conjugated polymers geometric model for three operations zones: **a** the first zone—containing 6 carbon atoms, **b** the second zone—intermediate with a polymer chain composed of 10 carbon atoms and **c** the third zone—presenting 20 carbon atoms in its structure. **d**, **e** and **f** have the molecular orbital in the region of HOMO and LUMO under the null voltage of the devices, respectively

thus explaining the Coulomb blockage in molecular junctions [15] and the influence due to the geometry of the electrodes [16].

We have obtained the transport properties for a series of one-dimensional structures (1D) and have even quantities of carbon atoms starting with six (6), ten (10) and twenty (20) atoms in a single molecule (Fig. 1).

The stability of the chain with respect to single- and double-bond alternation is ensured by the sulfur atom belonging to the thiol group (–SH) connected at its ends forming a bridge with gold electrodes. In addition, the thiol-capped chains make a strong chemisorptions bond onto the metallic electrodes [17–23].

These devices are subject to two conditions:

(a) first at low voltages ranging from 0 to 0.1 V;
(b) and second at high voltages from 0 to 1.0 V.

The influence of the voltage parameters on the I–V characteristic is sensitive to quantum interference effects obtained in the (a) low voltage and is insured due to antiresonance in the transmission spectrum. In (b) high-voltage regime, we observe resonance tunneling-type conduction (Fig. 2) at this case the resonance takes to the current increase operating with similarity of Field Effect Transistor (FET) [24].

As a reference, we compare the electric characteristic result for (a) and (b) conditions and we focus on over a voltage 0 to 0.1 V for the low-voltage regime and for range $0 < V < 0.1$ V inside high-voltage regime.

We find characteristic of the electronic transport qualitatively different as the molecule is submitted to low and high voltage, highlight the absence or presence of quantum interference.

2 Materials and methods

The electronic transport properties were investigated by means of calculations based in the non-equilibrium Green's function (NEGF) method combined with the extended Hückel theory (EHT), a semi-empirical approach to the electron transport model.

Quantum interference has been predicted in the characteristic transmission of Huckel models designed to represent molecular systems [9,10,15,25,26].

The chains were optimized via the Extended Huckel method [27] on a free thiol group at an electronic temperature of 300 K and energy values obtained very close to the physical energies at 0 K. Although not the physical temperature of the system, the integration method for the Brillouin zone in metals proposed by Methfessel and Paxton [28] guarantees

an exponential convergence. To ensure optimal performance, the choice of polymers with higher homogeneity, stability, better organization of the chains, reproducibility and higher conductivity values were taken into account in this study.

The second part is the calculation of the transport properties of the optimized molecule being positioned perpendicularly between two fcc electrodes oriented along the (100) direction in a gold tip scanning tunneling microscope (STM) [29].

Where the surfaces of the upper atom (Au) at the STM point are connected at fixed distance by connecting the atom (Au) and (S) at a distance of 2.45A°.

Using the Green's functions of non-equilibrium and the Landauer–Büttiker equation [30,31] to calculate the current through the molecular junction being described as a function of the applied polarization given by:

$$I_{\mathrm{LR}}(V) = \frac{2e}{h}\int_{-\infty}^{+\infty} \mathrm{d}\varepsilon T_{\mathrm{LR}}(\varepsilon)\left[f(\varepsilon-\varepsilon_{\mathrm{L}}) - f(\varepsilon-\varepsilon_{\mathrm{R}})\right]. \quad (1)$$

where ε is the energy of scattering states from the electrodes, $f(\varepsilon-\varepsilon_{\mathrm{L}})$ and $f(\varepsilon-\varepsilon_{\mathrm{R}})$ denote Fermi distributions. The $T_{\mathrm{LR}}(\varepsilon)$ for the (left–right) electrode is the electron transmission probability incident to an energy ε through the device under the potential V bias. The difference between the electrochemical potentials in the left and right electrodes can be written as $\varepsilon_{\mathrm{L}} - \varepsilon_{\mathrm{R}} = eV$, were $\varepsilon_{\mathrm{L}} = E_{\mathrm{F}} + \frac{eV}{2}$ and $\varepsilon_{\mathrm{R}} = E_{\mathrm{F}} - \frac{eV}{2}$, respectively. To define the probability of electron transmission through the device starting from the left electrode (L) to the right (R) as a function of energy, we have obtained the transmission function $T(E, V)$ by an expression given by:

$$T(E) = Tr\left[\Gamma_{\mathrm{L}} G \Gamma_{\mathrm{R}} G^{+}\right]; \quad (2)$$

$T(E)$ is the total transmission and is a function applied to each power system level with G and G^{+} as the latest and advanced Green functions, respectively, describing the dynamics of electrons in the scattering region in which we analyze the influence of quantum interference phenomenon on the transport for the devices subjected to low and high voltages.

This methodology proved to be highly reliable in calculating the current–voltage characteristics, transmittance and the differential conductance of the system describing the transport properties of electronic devices for single molecules [30].

3 Results and discussion

Figure 2a shows the I–V curve in the high-voltage regime for the 6-carbon chain. A linear relationship is verified at $0 < V < 0.26$. For $0.26 < V < 0.41$, the device does not linearly depend on the voltage, so at $0.42 < V < 0.65$ we obtain a design of a FET device and a negative differential resonance emerges with a minimum value of 0.72 V.

Experimentally, Kyoungja Seo and Hyoyoung Lee [32] demonstrated electron transport changes in alkanethiol molecular junctions for voltage up to 0.6 V. However, in our work we obtained NDR for window larger than 0.7 V.

Figure 2a has a similar characteristic as regular FET devices. The conduction behavior for different chain sizes implies in the charge mobility through the overlapping of π-orbitals [33]. Demonstrating that single molecules can work as reproducible circuit elements [34] with regions of charge accumulation and/or depletion reached by external bias [35].

Also for high voltage, the inset in Fig. 2a shows the same current in the linear region at the limit of $0 < V < 0.1$ V.

In Fig. 2b, the I–V curve is obtained under the low-voltage regime, i.e. the system is subjected to a new voltage ranging from 0 to 0.1 V, the black ellipses indicate the occurrence of quantum interference within of the linear regime for low voltage.

Finally, in Fig. 2c we compared the inset of Fig. 2a in the high-voltage regime with the calculated low-voltage current of Fig. 2b.

We note the inset in Fig. 2c where clearly the destructive quantum interference on the low-voltage I–V curve is indicated by an ellipse and shows the difference in the transport characteristic according to the voltage regime at which the system is subject.

Figure 3a–f displays plots of the current I–V and conductance G–V chains for $N = 6$, 10 and 20 carbons revealing dramatic differences.

The transport efficiency depends on parameters such as the molecular length already observed experimentally [36], the transport is dominated by high levels of transmission in π-type conjugated molecules [37].

In fact, the conductance increases in the short-chain system and decreases for larger chains, in Fig. 3a the higher conductance was observed when compared with Fig. 3c and e, this performance is identical for two distinct regimes: low voltages ranging from 0 to 0.1 V and then at higher voltages, from $0 < V < 0.1$ V.

The theoretical and experimental results for quantum transport within the linear regime are of the direct tunneling type and are in accordance with a low electric bias (< 0.5 V) [38].

In the linear regime, the current tends to become unstable with increasing V. Correspondingly, a numerical differential

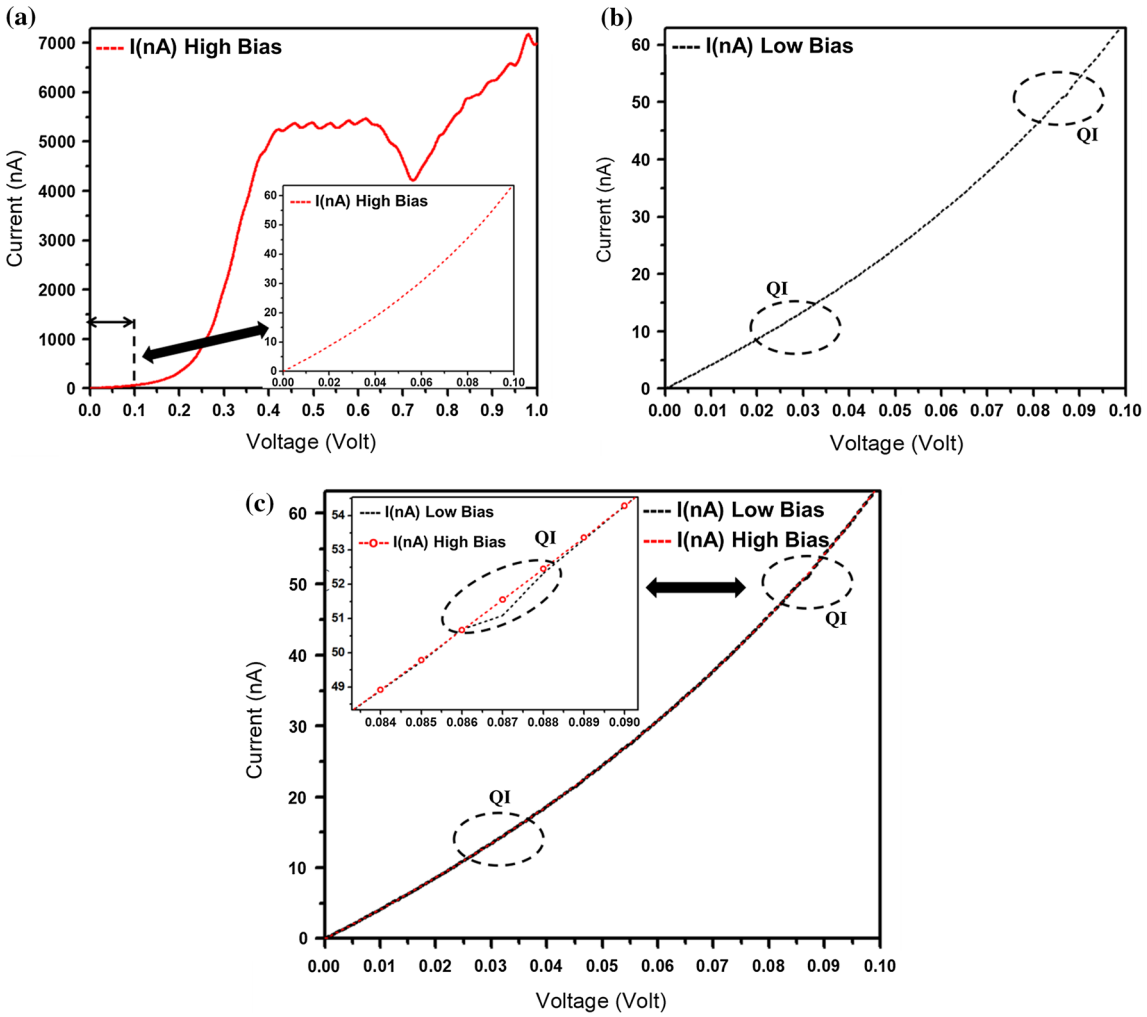

Fig. 2 In **a** the curve of the current under high voltage (0–1.0) for the chain containing 6 carbon atoms shown in solid line in red with a high-voltage curve inset within the linear range ($0 < V < 0.1$ V). In **b**, we calculated the I–V in the linear range ($0 < V < 0.1$ V) for low voltage (black dotted line). In **c**, we will have the destructive quantum interference on the I–V curve indicated by a black ellipse in the low-voltage curve (dotted line with red) with an insert displaying the specific interval of occurrence of the phenomenon of destructive quantum interference (Color figure online)

conductance exhibits considerable fluctuations of magnitude in low-voltage regimes showing the sensitivity in the three chains investigated Fig. 3b, d and f.

Particularly, the number of oscillations in G–V for low voltage is clearly attributed to the antiresonance phenomena when the conducting channel is blocked by backscattering. However, in the high-voltage regime this fluctuation spectrum is not manifested.

The transmission functions for 6, 10 and 20 carbon chains have similar shapes in the region near the Fermi level. In this region, the transport of electrons is dominant, where the mechanism can be interpreted in terms of transmission spectrum and spatial distribution of the molecular orbital's frontier shown in Fig. 1d, e and f [39].

In the following, the $T(E, V)$ transmission is shown which may give us a clear understanding of the electron transport behavior and the respective contour map illustrating the transmission peaks and QI signatures: (Figs. 4, 5 and 6).

In Fig. 4a at the high-voltage ($0 < \mathrm{V} < 0.1$ V) transmission channel around the Fermi level is increasing tightly for the entire voltage range. Next the $T(E, V)$spectrum in Fig. 5a shows the transmission appearing at around the Fermi level from -0.8 to 0.5 energy range and near $\mathrm{E_F}$ at 0.8 V.

In Fig. 6a, the transmission coefficient appears below Fermi $\mathrm{E_F}$ energy; as a consequence, the current curve is smaller.

We complement these findings with transmission map 2-D Figs. 4b, 5b and 6b.

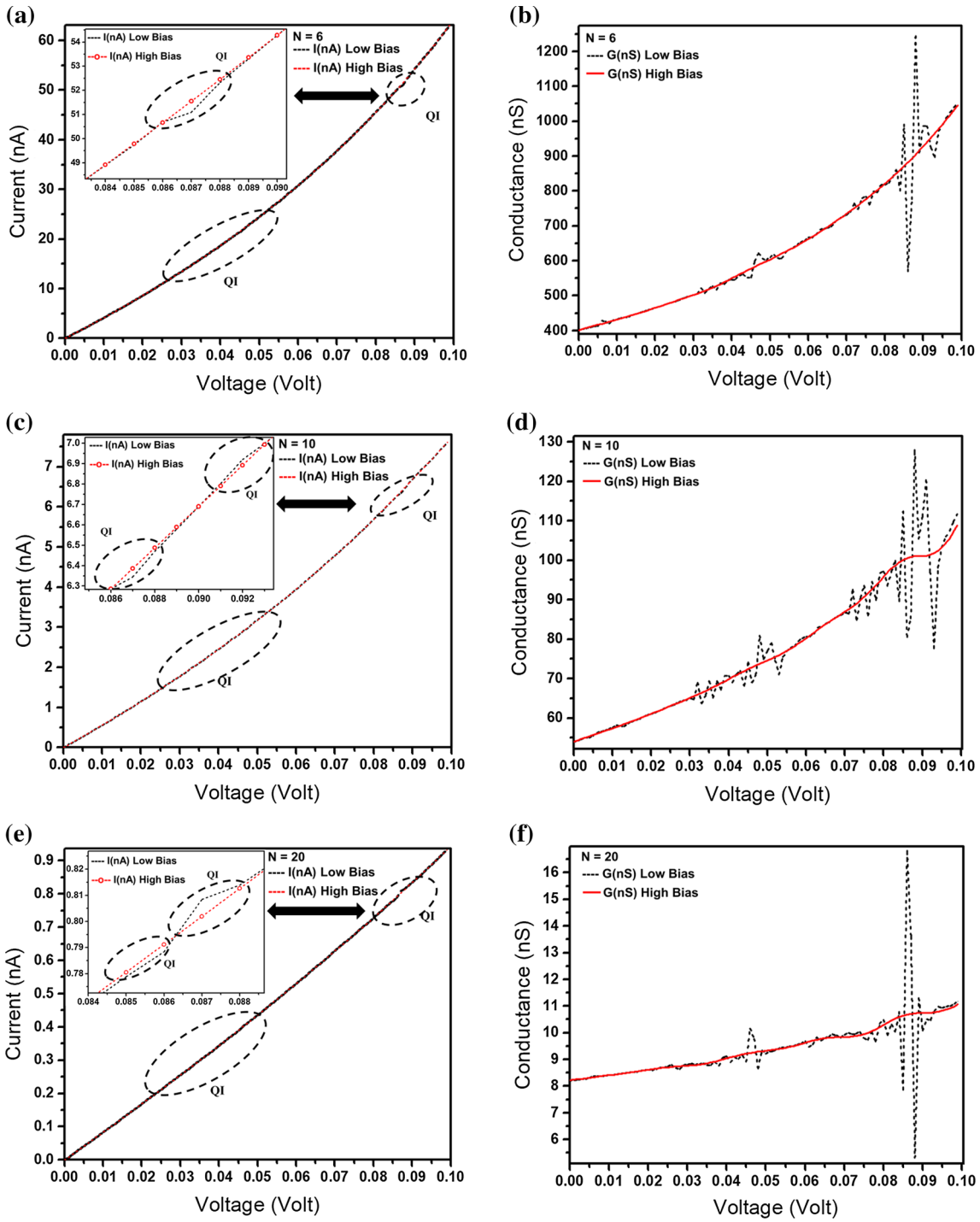

Fig. 3 The I–V characteristics for molecular chains with $N = 6, 10$ and 20 carbons are shown in **(a)**, **(c) and (e)**. Note that the low-voltage curves (shown in dotted black) and high-voltage curves (represented by a red dotted line) have insets indicating the phenomenon of quantum interference indicated by a black dotted ellipse. In **b**, **d** and **f**, we have the conductance at low voltage (solid line in black) and high voltage (solid line in red) with localized oscillations visible in low-voltage curves around $0.035 < V < 0.055$ and $0.075 < V < 0.095$ V (Color figure online)

The results of $T(E, V)$ in low-voltage regimes are presented in Figs. 7, 8 and 9, and they are in general rather similar to those of in high-voltage regimes.

In Fig. 7a, the high transmission channel closes the Fermi level for the whole voltage range and the current increases.

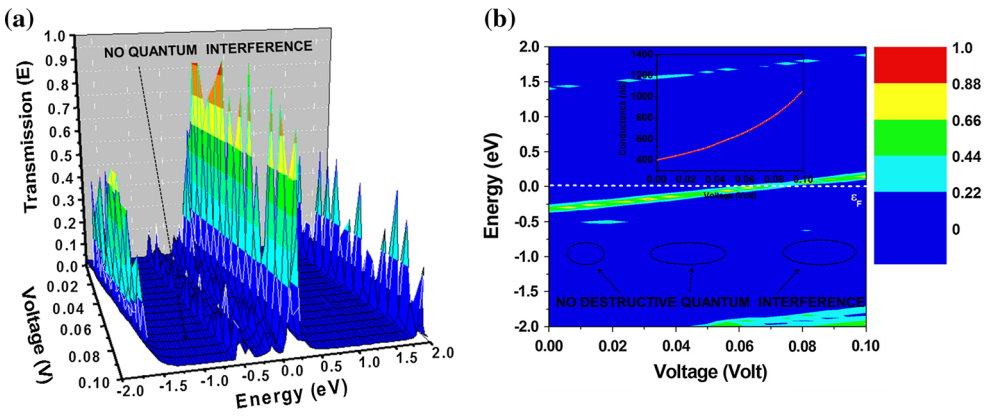

Fig. 4 In **a**, the 3-D graph illustrating the transmission spectrum as a function of energy and voltage, $T(E, V)$ illustrates the energy band with no destructive quantum interference with a black dotted arrow, while in **b** the respective 2-D map contour and the inset conductance graphic in the color red for the chain containing 6 carbon atoms (Color figure online)

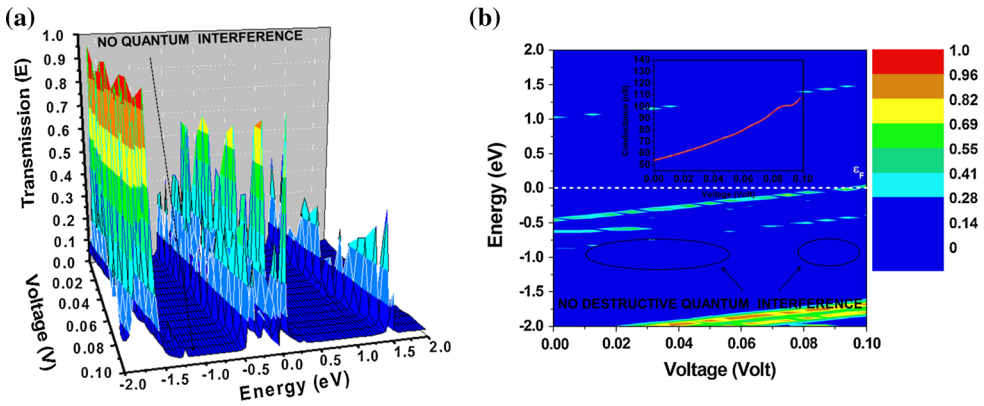

Fig. 5 In **a**, the 3-D graph illustrating the transmission as a function of energy and voltage $T(E, V)$ with a black dotted arrow illustrates the energy band with no destructive quantum interference, while in **b** the respective 2-D map contour and the inset conductance graphic in the color red for the chain containing 10 carbon atoms (Color figure online)

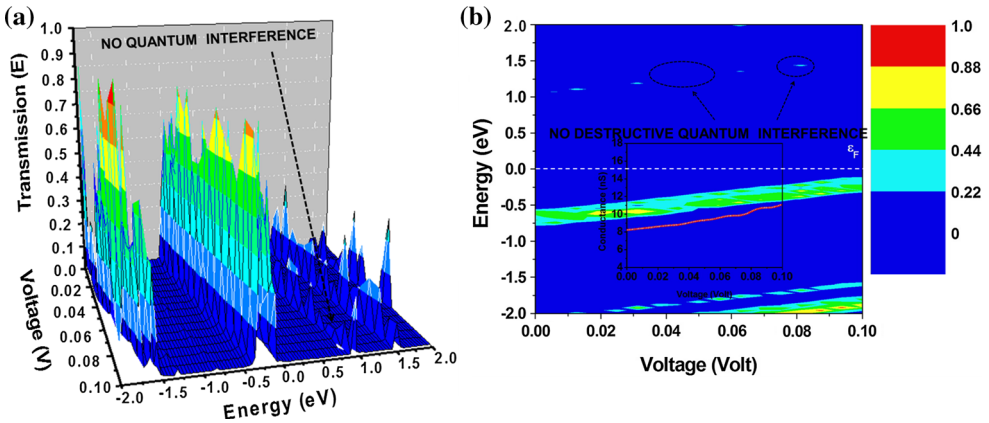

Fig. 6 In **a**, the 3-D graph illustrating the transmission as a function of energy and voltage $T(E, V)$ with a black dotted arrow illustrates the energy band with no destructive quantum interference, while in **b** the respective 2-D map contour and the inset conductance graphic are in the color red for the chain containing 20 carbon atoms (Color figure online)

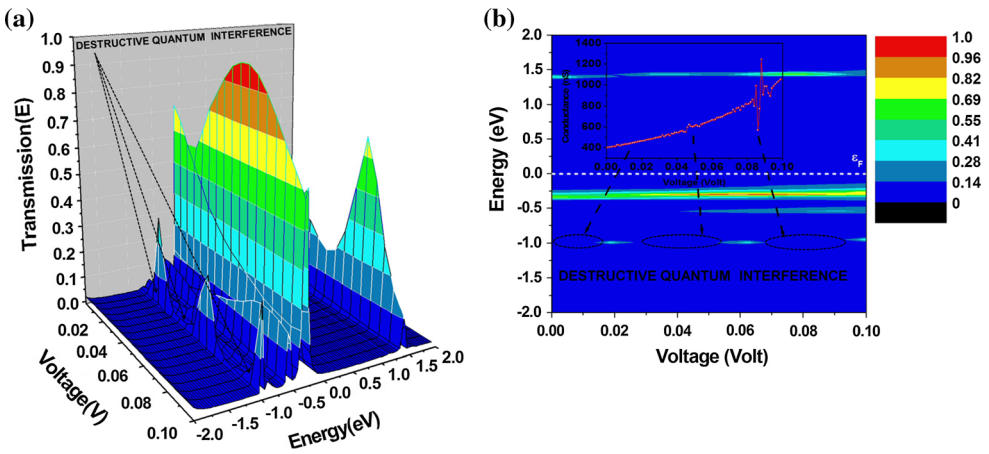

Fig. 7 In **a**, a 3-D graph illustrating the transmission $T(E, V)$ with a dotted arrow shows local destructive quantum interference, while at Fig. 3, the bottom panel of the 2-D map contour with miniature conductance graphic in red color with dotted arrows illustrates the range of voltage, and energy with destructive quantum interference is demarcated by a dotted ellipse in black color for the chain containing 6 carbon atoms with destructive quantum interference in turn of the 0.013, 0.035 and 0.075 V for a energy − 1.0 eV level (Color figure online)

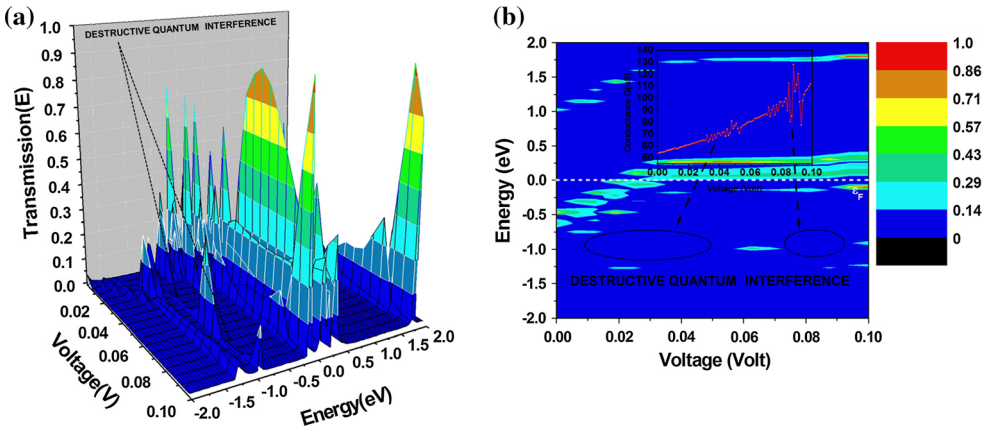

Fig. 8 In **a**, a 3-D graph illustrating the transmission $T(E, V)$ with a dotted arrow shows local destructive quantum interference, while in **b** the bottom panel of the 2-D map contour with miniature conductance graphic in red color with dotted arrows illustrating the range of voltage, and energy with destructive quantum interference is demarcated by a dotted ellipse in black color for the chain containing 10 carbon atoms with destructive quantum interference in turn of the 0.035 and 0.075 V for a −1.0 eV energy level (Color figure online)

The transmission spectrum in Fig. 8a appears at around the Fermi from a − 1.0 to 1.0 eV energy range the newly opened channels move the bias window.

In Fig. 9a shows that the N = 20 elongation has influence on the transmission peaks above the Fermi level and contributed to the quantum scattering in the voltage ranges 0.035 and 0.075 V for the energy level 1.25 eV.

Results in low voltage in Fig. 7a for a − 1.0 eV energy level and ranging from $0.035 < V < 0.055$ and $0.075 < V < 0.095$ V show the transmission peak is rapidly suppressed.

In Fig. 8a, the transmission peak is suppressed in the same bias voltage at a − 1.0 to − 0.8 eV energy range.

The transport in Fig. 9a for level energy LUMOs 1.5 at 1.0 eV contributes to transport, and again the transmission peak is suppressed at about 1.25 eV. Thus, the antiresonance reduces the transmission probability leading to the appearance of oscillations detected in the G–V curve [see New Fig. 3b, d and f].

In the 2-D map we indicated the regions in which the destructive quantum interference is notorious and these oscillations in G–V curve are related to the transmittance spectrum of Figs. 7, 8 and 9.

In general, this result suggests that the transmittance in low-bias regime of 0–0.1 V, the energy of the electron transport is close to the energy of the molecular level and the electron wave is trapped in the levels reflecting front and back between the junctions in such a manner as to produce destructive interference for specific voltages.

These findings agree very well with the electrical tension as an important energy scale for the dynamics, where

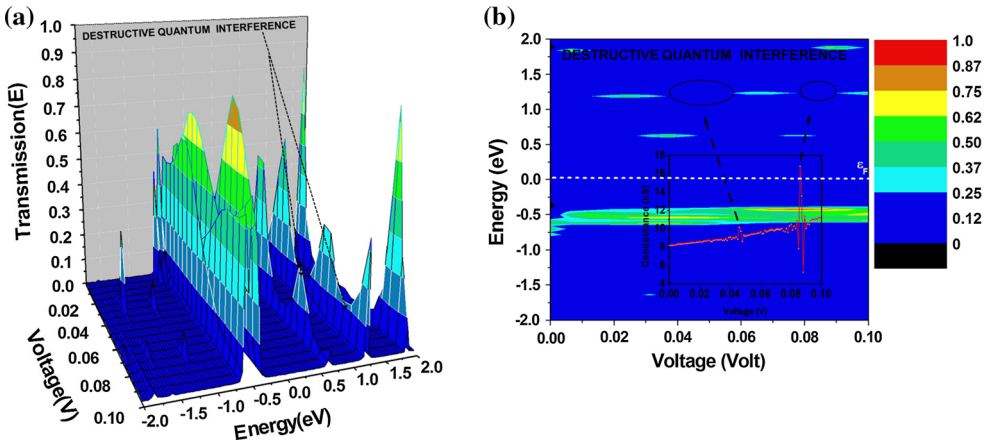

Fig. 9 In **a**, a 3-D graph illustrating the transmission $T(E, V)$ with a dotted arrow shows local destructive quantum interference, while at **b** the bottom panel of the 2-D map contour with miniature conductance graphic in red color with dotted arrows illustrating the range of voltage, and energy with destructive quantum interference is demarcated by a dotted ellipse in black color for the chain containing 20 carbon atoms with destructive quantum interference in turn of the 0.035 and 0.075 V for 1.25 eV energy level (Color figure online)

the oscillations appear and that can be originated due to the short relaxation time of the molecule coming accompanied by oscillatory behavior [40].

4 Conclusion

In this work, electron transport is shown to be mostly ballistic even at low voltages of 0–0.1 V. The non-equilibrium Green's function method coupled with the extended Hückel theory (EHT) has been used to calculate the electronic transport in order to investigate the relationship between the line shape of the conductance spectra and the length of the molecule chains.

The QI features in the transmission spectra, such as antiresonance, could be detected using the simple steps in window bias for low in of 0–0.1 V. The destructive interference disappears in the range to $0 < V < 0.1$ V; however, for larger voltages a FET without gate is characterized (i.e., only one operational window).

The analysis of the principal oscillations present in the calculated transmission spectra reveals that the electron transport changes in alkanethiol demonstrated quantum interference phenomena.

This results will help to understand the essential physics of the quantum effects of ballistic conduction present in molecular wires, as well as the parameters responsible for producing or contributing to the appearance (arising) of destructive quantum interference under low-voltage regime of 0–0.1 V.

The experimental result reported suggests the use of quantum oscillations as a valuable molecular signature for single-molecule identification for example, via electric current noise [41]. For low voltages, the almost ballistic nature of electron transport can be explained by considering the effects of the elastic and/or inelastic processes that occur in the transmission of electrons through single atom bonds and molecules.

Acknowledgements Alexandre de Souza Oliveira, and Antônio Thiago Madeira Beirão are grateful to CAPES—PROGRAM PRODOUTORAL/UFPA, CAPES/FAPESPA fellowship, respectively. Shirsley. S. da Silva and Jordan Del Nero would like to thank CNPq and INCT/Nanomateriais de Carbono for financial support.

References

1. Dimitrakopoulos, C.D., Mascaro, D.: Organic thin-film transistors: a review of recent advances. IBM J. Res. Dev. **45**, 11 (2001). https://doi.org/10.1147/rd.451.0011
2. Zhang, Y., Pena, J., Ambily, S., Shen, Y., Ralph, D.M.: 30 nm channel length pentacene transistors. Adv. Mater. **15**, 1632–1635 (2003). https://doi.org/10.1002/adma.200305202
3. Reed, M.A.: Molecular-scale electronics. Proc. IEEE **87**, 652–658 (1999). https://doi.org/10.1109/5.752520
4. Aviram, A., Ratner, M.A.: Molecular rectifiers. Chem. Phys. Lett. **29**, 277–283 (1974). https://doi.org/10.1016/0009-2614(74)85031-1
5. Del Nero, J., Laks, B.: Effect of Bipolaron type of defect on the polyacetylene-polycarbonitrile copolymer. Synth. Metals **84**, 869–870 (1997). https://doi.org/10.1016/S0379-6779(96)04187-2
6. Leal, J.F.P., Silva, S.J.S., Granhen, E.R., Silva Júnior, C.A.B., Moreira, M.D., Achete, C.A., Capaz, R.B., Del Nero, J.: Properties of charged defects on unidimensional polymers. J. Comput. Theor. Nanosci. **8**, 1–9 (2011). https://doi.org/10.1166/jctn.2011.1720
7. Beebe, J.M., Engelkes, V.B., Miller, L.L., Frisbie, C.D.: Transition from direct tunneling to field emission in metal-molecule-metal junctions. Phys. Rev. Lett. **97**, 026801–4 (2006). https://doi.org/10.1103/PhysRevLett.97.026801
8. Fujihira, M., Suzuki, M., Fujii, S., Nishikawa, A.: Currents through single molecular junction of Au/hexanedithiolate/Au measured by repeated formation of break junction in STM under UHV: effects

of conformational change in an alkylene chain from gauche to trans and binding sites of thiolates on gold. Phys. Chem. Chem. Phys. **8**, 3876–3884 (2006). https://doi.org/10.1039/b604945c
9. Baer, R., Neuhauser, D.J.: Phase coherent electronics: a molecular switch based on quantum interference. J. Am. Chem. Soc. **124**, 4200–4201 (2002). https://doi.org/10.1021/ja016605s
10. Walter, D., Baer, R., Neuhauser, D.J.: Quantum interference in polycyclic hydrocarbon molecular wires. Chem. Phys. **299**, 139–145 (2004). https://doi.org/10.1016/j.chemphys.2003.12.015
11. Emberly, E.G., Kirczenow, G.: State orthogonalization by building a Hilbert space: a new approach to electronic quantum transport in molecular wires. Phys. Rev. Lett. **81**, 5205–5208 (1998). https://doi.org/10.1103/PhysRevLett.81.5205
12. Akkermans, E., Montambaux, G.: Mesoscopic physics of electrons and photons, 1st edn, pp. 396–424. Cambridge University Press, Cambridge (2007)
13. Nitzan, A.: Electron transmission through molecules and molecular interfaces. Annu. Rev. Phys. Chem. **52**, 681–750 (2001). https://doi.org/10.1146/annurev.physchem.52.1.681
14. Granhen, E.R., Reis, M.A.L., Souza, F.M., Del Nero, J.: Transport model of controlled molecular rectifier showing unusual negative differential resistance effect. J. Nanosci. Nanotechnol. **10**, 1–6 (2010). https://doi.org/10.1166/jnn.2010.3018
15. Walczak, K.: The role of quantum interference in determining transport properties of molecular bridges. Cent. J. Chem. **2**, 524–533 (2004). https://doi.org/10.2478/BF02476205
16. Osorio, E.A., Moth-Poulsen, K., Van der Zant, H.S.J., Paaske, J., Hedegård, P., Flensberg, K., Bendix, J., Bjørnholm, T.: Electrical manipulation of spin states in a single electrostatically gated transition-metal complex. Nano Lett. **10**, 105–110 (2010). https://doi.org/10.1021/nl9029785
17. Xu, B., Xiao, X., Tao, N.J.: Measurements of single-molecule electromechanical properties. J. Am. Chem. Soc. **125**, 16164 (2003). https://doi.org/10.1021/na038949j
18. Haiss, W., Martin, S., Leary, E., Zalinge, H.V., Higgins, S.J., Bouffier, L., Nichols, R.J.: Impact of junction formation method and surface roughness on single molecule conductance. J. Phys. Chem. C. **113**, 5823 (2009). https://doi.org/10.1021/jp811142d
19. Haiss, W., Zalinge, H.V., Higgins, S.J., Bethell, D., Höbenreich, H., Schiffrin, D.J., Nichols., R.J.: Redox state dependence of single molecule conductivity. J. Am. Chem. Soc. **125**, 15294 (2003). https://doi.org/10.1021/ja038214e
20. Beebe, J.M., Kim, B., Gadzuk, J.W., Frisbie, C.D., Kushmerick, J.G.: Transition from direct tunneling to field emission in metal-molecule-metal junctions. Phys. Rev. Lett. **97**, 026801 (2006). https://doi.org/10.1103/PhysRevLett.97.026801
21. Li, C., Pobelov, I., Wandlowski, T., Bagrets, A., Arnold, A., Evers, F.: Charge transport in single Au/alkanedithiol/Au junctions: coordination geometries and conformational degrees of freedom. J. Am. Chem. Soc. **130**, 318 (2008). https://doi.org/10.1021/ja0762386
22. Horiguchi, K., Tsutsui, M., Kurokawa, S., Sakai, A.: Electron transmission characteristics of Au/1,4-benzenedithiol/Au junctions. Nanotechnology **20**, 025204 (2009). https://doi.org/10.1088/0957-4484/20/2/025204
23. Xiao, X., Xu, B., Tao, N.J.: Measurement of single molecule conductance: benzenedithiol and benzenedimethanethiol. Nano Lett. **4**, 267 (2004). https://doi.org/10.1021/nl035000m
24. De Lima, D.B., Reis, M.A.L., De Souza, F.M., Del Nero, J.: A general rule for nanoelectronic push-pull devices based on source-bridge-drain. J. Comput. Theor. Nanosci. **5**, 1–4 (2008). https://doi.org/10.1166/jctn.2008.016
25. Kala, C.P., Priya, P.A., Thiruvadigal, D.J.: Semiempirical study of electron transport of heterocyclic molecule based molecular device. J. Comput. Theor. Nanosci. **10**, 213–217 (2013). https://doi.org/10.1166/jctn.2013.2681
26. Markussen, T., Stadler, S., Thygesen, K.S.: The relation between structure and quantum interference in single molecule junctions. Nano Lett. **10**, 4260–4265 (2010). https://doi.org/10.1021/nl101688a
27. Pinheiro, F.A., Da Silva, S.J.S., Granhen, E.R., Del Nero, J.: Electronic transport in biphenyl single-molecule junctions with carbon nanotubes electrodes: the role of molecular conformation and chirality. Phys. Rev. B. **81**, 115456 (2010). https://doi.org/10.1103/PhysRevB.82.085402
28. Methfessel, M., Paxton, A.T.: High-precision sampling for brillouin-zone integration in metals. Phys. Na. B Condens. Matter Mater. Phys. **40**(6), 3616 (1989). https://doi.org/10.1103/PhysRevB.40.3616
29. Gerhard, L., Edelmann, K., Homberg, J., Valásek, M., Bahoosh, S.G., Lukas, M., Pauly, F., Mayor, M., Wulfheke, W.: Na electrically actuated molecular toggle switch. Nat. Commun. **8**(14672), 1–10 (2017). https://doi.org/10.1038/ncomms14672
30. Landauer, R.: Spatial variation of currents and fields due to localized scatterers in metallic conduction. J. Res. Dev. **1**, 223 (1957). https://doi.org/10.1147/rd.13.0223
31. Büttiker, M.: Four-terminal phase-coherent conductance. Phys. Rev. Lett. **57**, 1761 (1986). https://doi.org/10.1103/PhysRevLett.57.1761
32. Kyoungja, S., Hyoyoung, L.: Molecular electron transport changes upon structural phase transitions in alkanethiol molecular junctions. ACS Nano. **3**, 2469–2476 (2009). https://doi.org/10.1021/nn8008917
33. Dey, A., Singh, A., Das, D., Iyer, P.K.: Organic semiconductors: a new future of nanodevices and applications. In: Babu Krishna Moorthy, S. (ed.) Thin Film Structures in Energy Applications. Springer, Cham (2015). https://doi.org/10.1007/978-3-319-14774-1_4
34. Isshiki, Y., Matsuzawa, Y., Fujii, S., Kiguchi, M.: Investigation on single-molecule junctions based on current–voltage characteristics. Micromachines **9**(67), 1–15 (2018). https://doi.org/10.3390/mi9020067
35. De Lima, D.B., Del Nero, J.: Fundamental rules to construct highly integrated organic nanowires as nanodevices. J. Comput. Theor. Nanosci. **5**(7), 1–5 (2008). https://doi.org/10.1166/jctn.2008.035
36. Nacci, C., et al.: Conductance of a single flexible molecular wire composed of alternating donor and acceptor units. Nat. Commun. **6**, 7397 (2015). https://doi.org/10.1038/ncomms8397
37. Heeger, A.J.: Semiconduction and metallic polymers: the fourth generation polymeric materials. Rev. Mod. Phys. **73**, 681–700 (2001). https://doi.org/10.1103/RevModPhys.73.681
38. Seminario, J.M., Yan, L.: Ab initio analysis of electron currents in thioalkanes. I. J. Q. Chem. **102**, 711–723 (2005). https://doi.org/10.1002/qua.20384
39. Li, Y.W., Yin, G.P., Yao, G.H.: First-principles study of substituents effect on molecular junctions: towards molecular rectification. Comput. Mater. Sci. **42**, 638 (2008). https://doi.org/10.1016/j.commatsci.2007.09.018
40. Li, S., Huang, Guang-Yao, Guo, Jing-Kun, Kang, N., Caroff, P., Xu, Hong-Qi: Ballistic transport and quantum interference in InSb nanowire devices. Chin. Phys. B. **26**, 2 (2017). https://doi.org/10.1088/1674-1056/26/2/027305
41. Tsutsui, M., Taniguchi, M., Kawai, T.: Single-molecule identification via electric current noise. Nat. Commun. **138**, 1–5 (2010). https://doi.org/10.1038/ncomms1141